SIAM J. SCI. COMPUT.
Vol. 34, No. 2, pp. A993–A1009

ADAPTIVE SPECTRAL VISCOSITY FOR HYPERBOLIC CONSERVATION LAWS*

EITAN TADMOR† AND KNUT WAAGAN‡

Abstract. Spectral approximations to nonlinear hyperbolic conservation laws require dissipative regularization for stability. The dissipative mechanism must, on the other hand, be small enough in order to retain the spectral accuracy in regions where the solution is smooth. We introduce a new form of viscous regularization which is activated only in the local neighborhood of shock discontinuities. The basic idea is to employ a spectral edge detection algorithm as a dynamical indicator of where in physical space to apply numerical viscosity. The resulting spatially local viscosity is successfully combined with spectral viscosity, where a much higher than usual cut-off frequency can be used. Numerical results show that the new adaptive spectral viscosity scheme significantly improves the accuracy of the standard spectral viscosity scheme. In particular, results are improved near the shocks and at low resolutions. Examples include numerical simulations of Burgers' equation, shallow water with bottom topography, and the isothermal Euler equations. We also test the schemes on a nonconvex scalar problem, finding that the new scheme approximates the entropy solution more reliably than the standard spectral viscosity scheme.

Key words. nonlinear conservation laws, spectral viscosity, edge detection

AMS subject classifications. 35L60, 35L67, 65M70

DOI. 10.1137/110836456

1. Introduction—main ingredients.

Let $u(\cdot) : (-\pi, \pi) \mapsto \mathbb{R}$ be a 2π-periodic function, and let $u_N \equiv P_N u(x)$ denote its pseudospectral approximation of order N,

$$u_N(x) = P_N u(x) := \sum_{k=-N}^{N} \widehat{u}_k e^{ikx}, \qquad \widehat{u}_k = \sum_{j=-N}^{N} u(x_j) e^{-ikx_j} \frac{\Delta x}{2\pi}, \tag{1.1a}$$

which is based on the equidistant sample points

$$x_j = \left(j - \frac{1}{2}\right) \Delta x, \qquad \Delta x = \frac{2\pi}{2N+1}. \tag{1.1b}$$

If $u \in C^\infty$, the Fourier approximation enjoys infinite (i.e., spectral) order of accuracy. When applied to functions that are only piecewise smooth, however, this property breaks down even in the smooth regions. Around a discontinuity, $\mathcal{O}(1)$ Gibbs' oscillations are observed, and only first order convergence $\mathcal{O}(1/N)$ is obtained in the smooth regions. The spectral order of accuracy can be recovered by filtering techniques which

*Submitted to the journal's Methods and Algorithms for Scientific Computing section June 6, 2011; accepted for publication (in revised form) January 12, 2012; published electronically March 29, 2012. This research was supported in part by Office of Naval Research grants ONR N000140910385, N000141210318, and National Science Foundation grant DMS 10-08397.

http://www.siam.org/journals/sisc/34-2/83645.html

†Department of Mathematics, Center for Scientific Computation and Mathematical Modeling (CSCAMM), Institute for Physical Science and Technology (IPST), University of Maryland, College Park, MD 20742-4015 (tadmor@cscamm.umd.edu).

‡Department of Mathematics, Center for Scientific Computation and Mathematical Modeling (CSCAMM), Institute for Physical Science and Technology (IPST), University of Maryland, College Park, MD 20742-4015 (KWaagan@cscamm.umd.edu). Current address: Department of Applied Mathematics, University of Washington, Seattle, WA 98195 (kwaagan@wu.edu).

we will refer to as postprocessing [1, 6, 20]. Since the filtering requires explicit knowledge of the locations of singularities, algorithms for detecting edges from spectral data have been developed [3, 20].

We consider conservation laws

$$u_t + f(u)_x = 0, \qquad u(\cdot,t) : (-\pi,\pi) \mapsto \mathbb{R}, \tag{1.2}$$

subject to 2π-periodic initial data $u_0(x)$. A straightforward pseudospectral approximation of (1.2) takes the form

$$(u_N)_t + (P_N f(u_N))_x = 0. \tag{1.3}$$

Since solutions of (1.2) develop shock discontinuities at a finite time, Gibbs' phenomena will render the pseudospectral method (1.3) inaccurate or even unstable [16]. The instability can be addressed by the classical vanishing viscosity method, which is given by

$$(u_N)_t + (P_N f(u_N))_x = \epsilon_N (u_N)_{xx}, \quad \epsilon_N = \mathcal{O}(1/N). \tag{1.4}$$

It yields a stable scheme but obviously involves a first order error $\mathcal{O}(1/N)$. Thus, stability is gained at the expense of sacrificing spectral accuracy.

1.1. Spectral viscosity. In order to retain both high accuracy and stability, the spectral viscosity (SV) method was introduced in [16],

$$(u_N)_t + (P_N f(u_N))_x = \epsilon_N Q * (u_N)_{xx}, \quad Q(x) := \sum_{|k|\le N} \widehat{Q}_k e^{ikx}. \tag{1.5}$$

The coefficient ϵ_N represents the magnitude of diffusion and will be set to $\epsilon_N = \mathcal{O}(1/N)$. The viscosity kernel Q is chosen so as to filter out the large scales from the diffusion operator. Spectral accuracy is ensured by leaving enough large scale modes without dissipation, i.e., $\widehat{Q}_k = 0$ for $|k| < m$ with the cut-off frequency m increasing appropriately with N. We use

$$Q(x) = \sum_{|k|>m} \exp\left(-\left(\frac{N-k}{k-m}\right)^2\right) e^{ikx}, \tag{1.6}$$

and unless otherwise noted, we let $m = \sqrt{N}$, which results in a stable SV scheme (see, e.g., [12, 14, 16, 17, 19]). The resulting SV method reads

$$\text{SV} \mapsto (u_N)_t + (P_N f(u_N))_x = -N \sum_{|k|>m} \frac{k^2}{N^2} \widehat{Q}_k \widehat{u}_k(t) e^{ikx}, \widehat{Q}_k = \exp\left(-\left(\frac{N-k}{k-m}\right)^2\right). \tag{1.7}$$

The parameterization $m \sim \sqrt{N}$ corresponds to the second order diffusion in the vanishing viscosity regularization in (1.4). A more general setup, based on *hyperviscosity* of order $2s$, was introduced in [18],

$$\text{HyperSV} \mapsto (u_N)_t + (P_N f(u_N))_x = -N \sum_{|k|>m} \eta\left(\frac{|k|}{N}\right) \widehat{u}_k(t) e^{ikx}, \tag{1.8}$$

$$\eta(\xi) \ge \max\left\{\xi^{2s} - \frac{c}{N}, 0\right\}.$$

The case $s = 1$ corresponds to the usual SV method. As s increases, the resulting HyperSV is activated at smaller portions of the spectrum, $|k| > m \sim N^{(2s-1)/(2s)}$, and its stability was proved in [18]. In particular, this allows us to parameterize the cut-off m as a fixed fraction of N, which will be advocated below. In closing, we note that the SV and HyperSV methods have been generalized to nonperiodic problems in [11, 8, 10].

1.2. Postprocessing. As pointed out in [11, 15], the SV solution u_N is better viewed as an approximation to the Fourier projection $P_N u(\cdot, t)$ rather than to the exact solution $u(\cdot, t)$ itself. The total error,

$$u_N - u \equiv (u_N - P_N u) + (P_N u - u), \tag{1.9}$$

will therefore be dominated by the interpolation error $P_N u - u$ which is $\mathcal{O}(1/N)$ due to Gibbs' oscillations. Nevertheless, spectral accuracy of $P_N u$ can be recovered by postprocessing in smooth regions. Hence, we expect that spectral accuracy of the SV solution u_N can be recovered in the same way. Following [21, 23], a postprocessed SV solution, denoted $\widetilde{u}_N$, will be recovered from u_N by a convolution with a proper mollifier, $M(\xi)$,

$$\widetilde{u}_N(x) = \int_{-\infty}^{\infty} \frac{1}{\theta} M\left(\frac{x-y}{\theta}\right) u_N(y)\, dy, \qquad M(\xi) := \rho(\xi) D_p(\xi). \tag{1.10a}$$

Here, D_p is the usual Dirichlet kernel of degree p,

$$D_p(\xi) = \frac{\sin[(p+\frac{1}{2})\xi]}{\sin[\frac{1}{2}\xi]}, \tag{1.10b}$$

and ρ is the smooth weighting function locally supported in $[-\pi, \pi]$,

$$\rho(\xi) = \bar{\rho} \exp\left(-\frac{10\xi^2}{(\pi^2 - \xi^2)_+}\right), \tag{1.10c}$$

with the normalization factor $\bar{\rho}$ chosen so that ρ has unit mass,

$$\int_{-\infty}^{\infty} M(\xi)\, d\xi = 1. \tag{1.10d}$$

There are two parameters to be chosen:

1. The degree p in (1.10b) is set to be a fraction of N; we use $p = 0.5586\theta N$ as suggested in [23].
2. The scaling factor θ dictates the active neighborhood of mollification, $[x - \theta\pi, x + \theta\pi]$ in (1.10). Note that θ can depend on x. Indeed, we will take $\theta(x) = \mathrm{dist}(x, \mathcal{S}(u))/\pi$, where $\mathcal{S}(u)$ is the set of singular points of u. In the next section we describe an algorithm for finding $\mathcal{S}(u)$ from u_N.

1.3. Spectral edge detection. As seen in the previous section, postprocessing requires explicit knowledge of the spatial location of discontinuities. One needs to know the interval of smoothness surrounding each point x so that $\theta(x)$ in (1.10) can be computed. To this end, the locations, as well as the magnitudes, of discontinuities may be extracted from spectral data by using the following edge detection algorithm from [3, 4, 20]. Let $K(u_N)$ be the concentration kernel

$$K(u_N)(x) = \sum_{|k| \le N} \mathrm{sign}(k)\, \sigma_k \hat{u}_k e^{ikx}, \tag{1.11a}$$

where the so-called concentration factors, $\sigma_k \equiv \sigma(|k|/N)$, are normalized such that

$$\sum_{k=1}^{N} \frac{\sigma\,(k/N)}{k} = 1. \tag{1.11b}$$

The idea behind the concentration kernel is to provide a function $K(u_N)$ that vanishes in smooth regions of u and equals the (signed) magnitude of the jump discontinuity at the jump location. Here, we take the concentration kernel

$$\sigma(\xi) = \bar{\sigma}(1 - \cos \pi\xi), \tag{1.11c}$$

where (1.11b) determines the normalization factor

$$\bar{\sigma} = \left(\sum_{k=1}^{N} \frac{1 - \cos \frac{\pi k}{N}}{k} \right)^{-1}. \tag{1.11d}$$

This choice of σ yields an accurate localizer $K(u_N)$ that has some oscillations near the discontinuities.

In order to pinpoint the shock locations, the authors of [4] suggested a resolution-dependent lower threshold, above which $K(u_N)$-values signify a shock. They consider the enhanced spectral concentration kernel given by

$$K_\delta(u_N)(x) = \chi_\delta[K(u_N)], \tag{1.12a}$$

where

$$\chi_\delta[\xi] := \begin{cases} 0, & |\xi| \le \delta, \\ \xi, & |\xi| > \delta \end{cases} \tag{1.12b}$$

is a cut-off function parameterized by the cut-off magnitude δ. The cut-off δ will typically depend on N. The underlying assumption is that there is a scale separation between the shock magnitude and the local variation in the smooth data, and these scales should be reflected in the cut-off δ. This cut-off technique was used in [5] to provide shock locations for postprocessing, i.e., to specify θ in (1.10). In the next section we will introduce a new application of this shock detection method: We will use it as a *dynamical* indicator of where in physical space to activate spectral diffusion.

2. New algorithms—from edge detection to adaptive viscosity. Our basic intuition is that we want to avoid numerical diffusion in the smooth regions while ensuring that there is enough of it in the local neighborhood of shocks. To accomplish this we employ the localizer $K(u_N)$ as a local diffusion coefficient, letting

$$(u_N)_t + (P_N f(u_N))_x = \epsilon_N |K(u_N)| \cdot (u_N)_{xx}. \tag{2.1}$$

Note, however, that $K(u_N)$ need not be spectrally small in the smooth region, and hence (2.1) does not lead to a spectrally accurate scheme. In order to retain spectral accuracy in smooth regions we cut off the localizer K_N below a small threshold in the spirit of the enhanced edge detector (1.12b). Other factors may also make $K(u_N)$ unsuitable; for example, it will be oscillatory near the discontinuities.

Thus, in order to obtain a more suitable local diffusion coefficient we consider a modified localizer $L(u_N)$. The modification can be broken down into the following steps:

(i) First, we evaluate $|K(u_N)|$ to ensure a positive viscosity amplitude, as already indicated in (2.1).

(ii) Next, we truncate to enforce $|K(u_N)| \leq 1$, since we want to control the largest possible magnitude of the diffusion coefficient. Neglecting this may produce restrictions on the step size when discretizing in time.

(iii) We then mollify the result with a small width $\lambda = \mathcal{O}(1/N)$. This eliminates small scale oscillations in $K(u_N)$.

(iv) We renormalize so that the maximum of $\min(1, K(u_N))$ before mollification is retained, since that is the true measure of shock strength.

(v) Any value smaller than $\delta = \mathcal{O}(1/N)$ is set to 0. This cut-off is crucial, since $K(u_N)$ need not be spectrally small away from the discontinuities.[1]

The resulting modified localizer L_N reads

$$L(u_N) \equiv \chi_\delta[\, C\mu_\lambda * \min(|K(u_N)|, 1)], \tag{2.2a}$$

where C is a renormalizing constant so that step (iv) holds,

$$C = \frac{\| \min(|K(u_N)|, 1) \|_\infty}{\| \mu_\lambda * \min(|K(u_N)|, 1) \|_\infty}, \tag{2.2b}$$

the cut-off function χ_δ is given by (1.12b), and μ_λ is the mollification kernel

$$\mu_\lambda(x) = \frac{1}{\lambda} \exp\left(-\frac{10x^2}{(\lambda^2\pi^2 - x^2)_+} \right). \tag{2.2c}$$

Two N-dependent parameters remain to be specified. Throughout, we will take the mollification width $\lambda = 3\pi/N$, and the lower cut-off $\delta = \pi/N$.

2.1. Localized viscosity (LV). We define the localized viscosity (LV) scheme by

$$(u_N)_t + (P_N f(u_N))_x = \epsilon_N L(u_N) \cdot (u_N)_{xx}. \tag{2.3}$$

Hence this scheme amounts to the classical vanishing viscosity scheme (1.4) when $L(u_N)(x) \equiv 1$, i.e., at a discontinuity, and the inviscid scheme (1.3) when $L(u_N)(x)$ vanishes.

2.2. Localized spectral viscosity (LSV). Instead of the full viscosity term in (2.3), we could add a spectral viscosity. The result is the localized spectral viscosity (LSV) scheme

$$(u_N)_t + (P_N f(u_N))_x = \epsilon_N L(u_N)[Q * (u_N)_{xx}]. \tag{2.4}$$

This scheme switches between the spectral viscosity scheme (1.5) near discontinuities and the inviscid scheme (1.3) elsewhere. It is therefore less dissipative than both the LV and SV schemes and need not provide sufficient dissipation to control Gibbs' oscillations.

[1] Spectrally small amplitude of $K(u_N)$ in smooth regions can be achieved by using exponential concentration factors (page 1396) [4].

2.3. Adaptive spectral viscosity (ASV). Finally, we consider a scheme that switches between full viscosity near discontinuities and spectral viscosity in smooth regions. This is the adaptive spectral viscosity (ASV) scheme

$$(u_N)_t + (P_N f(u_N))_x = \epsilon_N L(u_N)(u_N)_{xx} + \epsilon_N \left(1 - L(u_N)\right)[Q * (u_N)_{xx}]. \tag{2.5}$$

Given the same choice of parameters, this scheme will be more dissipative than the SV, LV, and LSV schemes. However, for the ASV scheme we use larger values of the cut-off frequency m than with the other schemes, with $m = \frac{2}{3}N$ as a default choice.

More generally, one can let the choice of Q depend on u_N locally in space. This is only computationally efficient if a small number of coefficients Q is available; hence the ASV scheme (2.5) is a reasonable implementation of this idea, with the local dissipation given by either a standard SV choice of Q (1.6), the classical viscosity $\hat{Q}_k = 1$, or a linear combination of the two. A related application of the localizer was put forth in [22], where polynomial reconstruction of pointwise data was taken to as high order as possible while only using data from a smooth region.

2.4. Postprocessing. Independent of which type of viscous regularization is employed, we expect to have a situation analogous to the one described in section 1.2: The approximation error $u_N - u$ will be dominated by the $\mathcal{O}(1/N)$ representation error $P_N u - u$. Therefore, after computing $u_N(x,T)$ at a desired time $t = T$, we compute the postprocessed solution $\widetilde{u}_N(x,T)$ using (1.10) to recover spectral accuracy.

2.5. Time discretization. All of the above schemes are semidiscrete in the sense that they take the form of ODE systems in time. We discretize time with the strong stability-preserving explicit fourth order Runge–Kutta method [7]. Hence, formally we can only expect fourth order accuracy. At low enough resolutions, however, it may be that errors related to the spectral spatial approximation dominate, and hence one may still observe spectral accuracy in actual practice. The time step size is set to $\Delta t = 1/2N$ in all of our examples.

3. Convergence. In this section we prove the convergence of the ASV method (2.5). We begin by making reasonably simplifying assumption on the structure of the ASV parameters. The essence of the SV coefficients in (1.6) is that they vanish for small wavenumbers, $|k| < m$, and grow sufficiently fast to 1 for large wavenumbers; we will assume that $\widehat{Q}_k$ grow smoothly from 0 to 1 in the range of $m \le |k| \le 2m$:

$$\widehat{Q}_k = \varphi\left(\frac{|k|}{m}\right), \qquad \varphi(\zeta) = \begin{cases} 0, & |\zeta| < 1, \\ 1, & |\zeta| > 2. \end{cases} \tag{3.1}$$

A specific example outlined in (4.3) below reads $\varphi(\zeta) = \exp\big(-(2-\zeta)^2/(\zeta-1)^2\big)$. Letting $\widehat{R}_k := 1 - \widehat{Q}_k$, the ASV (2.5) is recast into the form

$$(u_N)_t + (P_N f(u_N))_x = \epsilon_N (u_N)_{xx} + \epsilon_N \left(1 - L(u_N)\right)[R * (u_N)_{xx}]. \tag{3.2}$$

The proof of convergence $u_N \to u$ is based on compensated compactness arguments (the div-curl lemma; see, e.g., [2]) along the lines of the convergence proofs for the SV method—consult [16, 18] and the references therein. To proceed with the proof of convergence, the following key a priori entropy production bound is sought:[2]

$$\epsilon_N \int_{t=0}^{T} \int_{x=-\pi}^{\pi} (\partial_x u_N)^2 dx dt \le Const_E. \tag{3.3}$$

[2]Here and throughout, we let *Const* denote various constants which may differ from case to case but are *independent of* N.

We shall sketch the proof of this estimate, which yields the following.

THEOREM 3.1. *Consider the ASV method* (2.5), (2.2) *with the viscosity coefficients* (3.1). *Set the SV parameters*

$$\epsilon = Const_Q \frac{1}{N}, \quad m = N^\theta, \ \theta < 1/2.$$

Assume that the ASV solution remains uniformly bounded, $\max_x |u_N(x,t)| \le Const_B$. *Then, for sufficiently large viscosity coefficient* $Const_Q$ *(depending on* f *and* $Const_B$*), the entropy bound* (3.3) *holds and, consequently,* u_N *converges to a weak solution of* (1.2), $u_N \to u$.

We remark that the single entropy bound (3.3) is sufficient to guarantee convergence in the case of general scalar fluxes (see, e.g., [24, 2]) and that the limit u is the unique entropy solution in the convex case [13].

To derive (3.3) we integrate (3.2) against u_N to find that the (quadratic) entropy production rate is given by

$$\frac{1}{2}\frac{d}{dt}\int_{-\pi}^{\pi} u_N^2(x,t)dx = -\overbrace{\epsilon_n \int_{x=-\pi}^{\pi} (\partial_x u_N)^2 dx}^{\mathcal{I}}$$
$$+ \overbrace{\int_{x=-\pi}^{\pi} u_N \big((I-P_N)f(u_N)\big)_x dx}^{\mathcal{II}} + \overbrace{\epsilon_N \int_{x=-\pi}^{\pi} u_N \left(1-L(u_N)\right)[R * (u_N)_{xx}]dx}^{\mathcal{III}}.$$

We need to show that the second and third terms do not interfere with the entropy dissipation in the first term. The second term is due to the *truncation error* of the spectral projection and can be upper-bounded in a standard fashion [16, 18],

$$\mathcal{II} = -\int_{x=-\pi}^{\pi} (\partial_x u_N)(I-P_N)f(u_N)dx \le Const_f \times \frac{1}{N}\int_{x=-\pi}^{\pi} (\partial_x u_N)^2 dx.$$

The third term is due to the adaptive spectral viscosity, and it does not exceed

$$\mathcal{III} \le \epsilon_N \left| \int_{x=-\pi}^{\pi} u_N \left(1-L(u_N)\right)[R * (u_N)_{xx}]dx \right|$$
$$\le \epsilon_N \max_x |u_N(x,t)| \int_{x=-\pi}^{\pi} |R * (u_N)_{xx}|\, dx.$$

We now come to the heart of the matter: since the last integrand, involving $\widehat{R}_k = 1-\varphi(|k|/m)$, is a trigonometric polynomial of degree $2m$ (any other multiple of m will do), its L^1 size cannot grow too large as a function of m:

$$\mathcal{III} \le \epsilon_N \, Const_B \, Const_R \times m^2. \tag{3.4}$$

We note in passing that instead of limiting the support of $\widehat{R}_k$ to $\mathcal{O}(m)$ modes, we can handle a more general class of SV parameters, where $\varphi(\zeta)$ increases sufficiently fast so that $\zeta(1-\varphi(\zeta))$ is decreasing; then, invoking [19, Lemma 2.1] yields the upper bound,

$$\mathcal{III} \le \epsilon_N \, Const_B \, Const_R \times m^2 \log(N),$$

which adds only an additional logarithmic factor to the upper bound (3.4).

We now combine the last few bounds to conclude that

$$\frac{1}{2}\frac{d}{dt}\int_{-\pi}^{\pi} u_N^2(x,t)dx \le -\epsilon_N \int_{x=-\pi}^{\pi} (\partial_x u_N)^2 dx + Const_f \times \frac{1}{N}\int_{x=-\pi}^{\pi} (\partial_x u_N)^2 dx + Const_{BR} N^{2\theta-1}\log(N).$$

The ASV parameterization guarantees that the last term decays to zero; time integration of the remaining terms yields

$$(Const_Q - Const_f)\,\frac{1}{N}\int_{t=0}^{T}\int_{x=-\pi}^{\pi} (\partial_x u_N)^2 dx \le \frac{1}{2}\int_{-\pi}^{\pi} u_N^2(x,0)dx + Const_T \times N^{2\theta-1}\log(N) := Const_E,$$

and (3.3) follows.

4. Numerical studies I. Scalar equations. We have presented four schemes that will be subject to numerical tests in this section. The schemes are SV (1.5) and LSV (2.4), both with cut-off frequency $m = \sqrt{N}$, ASV (2.5) with $m = \frac{2}{3}N$, and LV (2.3). Our goals are to identify schemes that maintain spectral accuracy when shocks develop and to compare the overall performance of the schemes relative to each other. For all of the examples, we use the viscosity coefficient $\epsilon_N = 4/N$.

4.1. Burgers' equation. Consider Burgers' equation $u_t + (\frac{1}{2}u^2)_x = 0$ subject to initial data

$$u_0(x) = 1 + \frac{1}{2}\sin(x). \tag{4.1}$$

The approximations u_N are sampled at $t = \pi$ at which time a shock has formed and is located at $x = 0$. The solution profiles are shown in Figure 1. While SV yields visible oscillations near the shock, LV yields a smoothed profile reminiscent of a TVD (total variation diminishing) scheme. For a more detailed study of accuracy, we plot the errors of the postprocessed solutions in Figure 2. SV can be seen to yield the expected spectral convergence. In comparison, the LV scheme is significantly more accurate near the shock and at low resolutions. However, its convergence eventually stagnates.

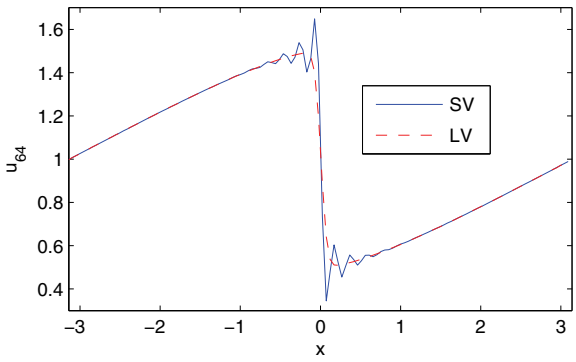

FIG. 1. *Solutions for Burgers' equation with smooth initial data.*

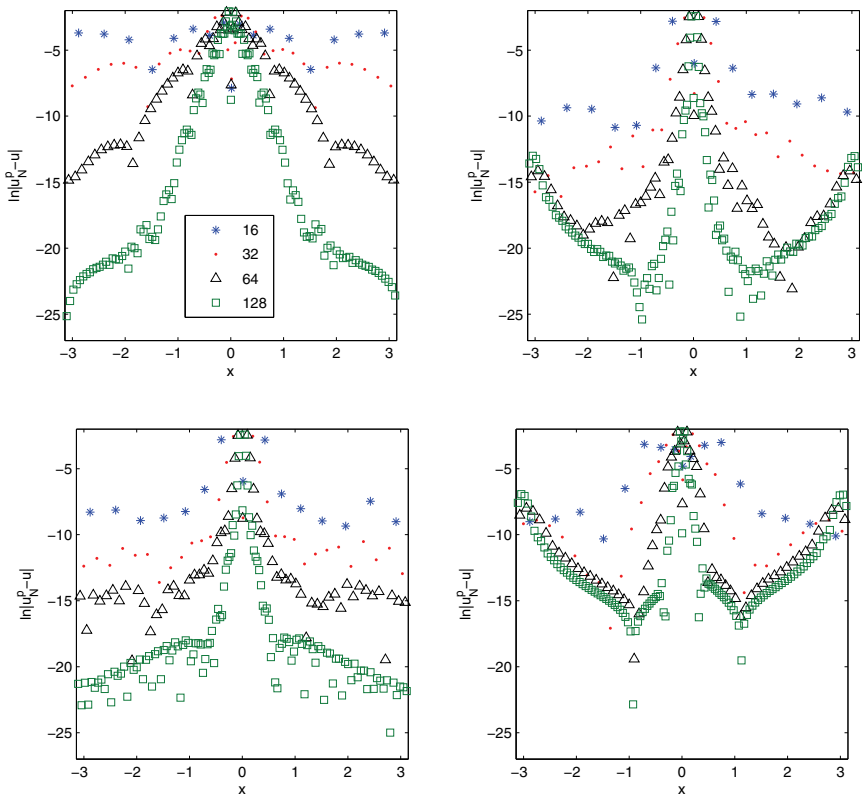

FIG. 2. *Burgers' equation with smooth initial data. Errors in postprocessed solutions* $\ln|\widetilde{u}_N - u|$ *at* $t = \pi$. *Top left: SV; top right: LV; bottom left: ASV; bottom right: LSV. The exact solution was calculated by characteristic tracing from the initial sample points.*

An explanation can be obtained from closely inspecting the solution profile: Although the LV scheme produces a near smooth shock profile, very small amplitude oscillations are still present in the smooth region, which could deteriorate performance at higher resolutions. Therefore, we turn to the ASV scheme as a compromise between local and spectral viscosity. Indeed, using ASV with cut-off at $m = \frac{2}{3}N$ keeps the diffusive zone around the shock narrow, as with LV, while removing the spurious oscillations. The result, as seen in Figure 2, is satisfactorily fast convergence comparable to SV, while we retain the improved efficiency of LV at low resolutions and near the shock. Finally, we test the LSV scheme. This scheme is clearly inferior to the others, in particular SV and ASV. Clearly too little dissipation is left in LSV after both spatial localization and spectral cut-off of viscosity.

4.2. Buckley–Leverett equation. Next, we consider the nonconvex Buckley–Leverett equation

$$u_t + \left(\frac{v^2}{v^2 + (1-v)^2}\right)_x = 0, \qquad v = \max(0, \min(1, u)). \tag{4.2}$$

This system is sensitive to what type of dissipative regularization is applied (see, e.g., [9]); i.e., different regularizations may converge to different weak solutions. First, we

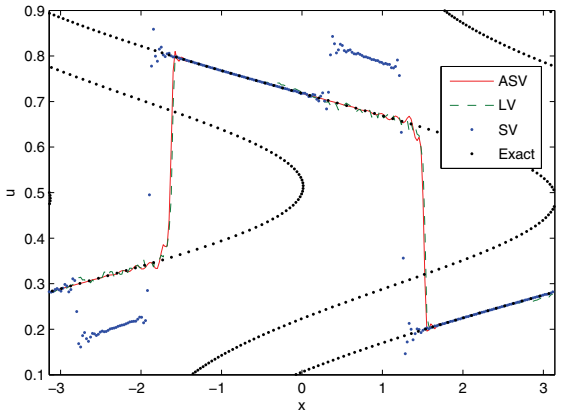

FIG. 3. *Solution profiles, initially smooth data for the Buckley–Leverett equation, $N = 128$, $t = \pi$. ASV (solid lines), LV (dashed lines), and SV (dots). We compare it to a multivalued solution based on tracing characteristics (dashed lines).*

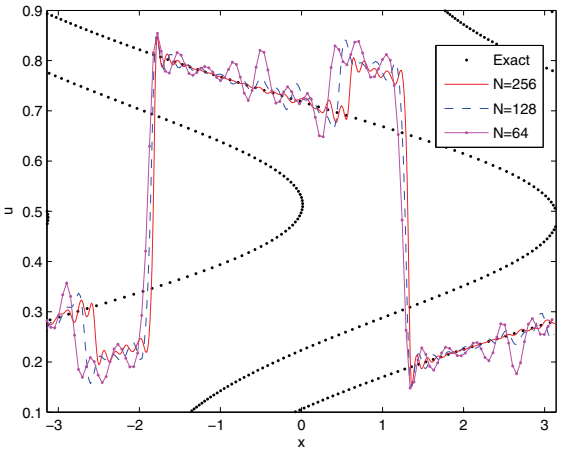

FIG. 4. *Solution profile, initially smooth data for the Buckley–Leverett equation. Refinement study of SV with Q given by* (4.3).

consider initial data $u(x,0) = \frac{1}{2} + \frac{1}{2}\sin(x)$. Figure 3 shows results at time $t = \pi$ after shocks were formed. The ASV and LV schemes produce stable, accurate results, much like in their performance in the convex case, while the SV scheme produces an apparently spurious solution. What appears to happen with SV is that the overshoots behind the shocks get interpreted as additional wave fronts. In order to look more closely at this phenomenon, we repeat this experiment with a different form of the SV filter Q, taking

$$\hat{Q}_k = \begin{cases} 0, & |k| \le m, \\ \exp(-(\frac{2m-k}{k-m})^2), & m < |k| < 2m, \\ 1, & 2m \le |k|. \end{cases} \tag{4.3}$$

This choice is based on [14], where a theoretical convergence rate of $1/2$ was obtained. The results with (4.3) and cut-off $m = \sqrt{N}$ are shown in Figure 4. The spurious wave

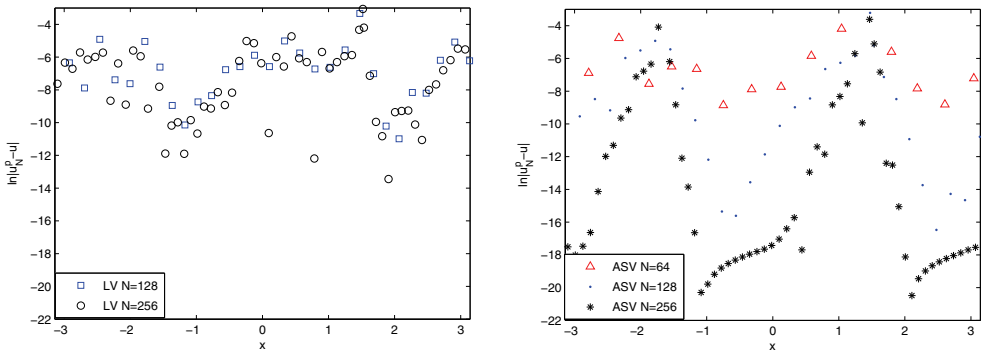

FIG. 5. *Errors, initially smooth data for the Buckley–Leverett. The LV method (left) versus the ASV method (right). The postprocessing was implemented with* $\theta(x) = \min(|x - 1.62|, |x + 1.52|)/\pi$.

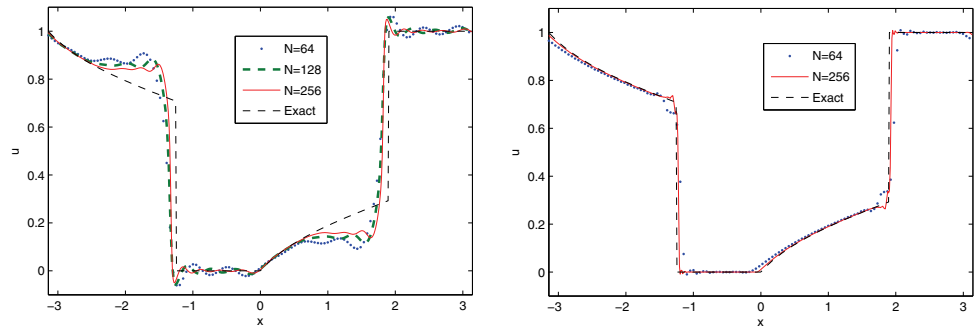

FIG. 6. *Riemann problem for Buckley–Leverett equation at* $t = \pi/2$. *The SV method (left) versus the ASV method (right).*

is still present, but it appears to vanish slowly with resolution, a tendency that is not clear with our standard choice of Q. Errors from the LV and ASV schemes are shown in Figure 5. The ASV scheme yields fast convergence, while LV does not perform satisfactorily upon this close inspection.

Next, we consider Riemann initial data with u jumping from 0 to 1. The entropy solution consists of a compound wave that can be expressed analytically. The ASV scheme approximates the entropy solution quite well (see Figure 6), except for small artifacts behind the shock that appear to vanish with resolution. The SV scheme only slowly approaches the entropy solution even when the more dissipative viscosity filter (4.3) is used; see Figure 6.

4.3. SV, ASV, and exponential filtering (EF). We conclude our discussion on the scalar problems by comparing various variants of SV solutions of Burgers' and Buckley–Leverett equations.

• *ASV versus SV.* For a more quantitative comparison of the ASV and SV schemes, we compute the average errors over all control points at least a distance 1 away from the shock; see Table 1. The observations based on the plots are confirmed. The more accurate behavior near the shock of the ASV scheme improves these error measures by orders of magnitude. We also provide error measures for alternative choices of cut-off frequencies m, which shows that they provide inferior results to their respective default values.

TABLE 1
Average error for checkpoints in $|x| \in [1, \pi]$.

	SV	ASV	ASV, $m = \sqrt{N}$	SV, $m = \frac{2}{3}N$
8	5.0e-2	1.6e-3	3.4e-3	4.7e-2
16	1.6e-2	2.3e-4	9.2e-4	1.4e-2
32	1.9e-3	9,4e-6	2.7e-4	7.4e-4
64	1.4e-5	4.3e-7	1.5e-5	3.4e-5
128	5.8e-8	3.6e-9	1.5-8	7.6e-7
256	4.2e-10	9.2e-13	1.0e-12	9.4e-9

• *SV versus EF.* A simple technique for reducing Gibbs' oscillation is to apply a low-pass filter at each computational step. As an example, consider the EF

$$E_N u := \sum_{k=-N}^{N} \widehat{u}_k \zeta\left(\frac{|k|}{N}\right) e^{ikx}, \quad \zeta(\xi) := e^{-\alpha\xi^p}, \tag{4.4}$$

with α and p positive parameters. In order to solve the conservation law (1.2), the exponential filter (4.4) applies at the end of each pseudospectral time step, $u_N(\cdot, t + \Delta t)$, yielding $E_N u_N(\cdot, t + \Delta t)$, which is used as input data for the next time step. Exponential filtering is, in fact, closely related to the SV method, (1.7). Indeed, one can address the SV method using an operator splitting, i.e., a pure transport step (1.3) followed by a pure SV step, using a specific choice of Q. The latter, "pure" SV problem reads

$$u_t = \epsilon Q * u_{xx}, \quad u(x, 0) = u_0, \tag{4.5}$$

whose solution is given by

$$\widehat{u}_k = (\widehat{u_0})_k e^{-\epsilon \widehat{Q}_k k^2 t}. \tag{4.6}$$

Thus, the filtering step in the EF method (4.4) corresponds to solving the SV step (4.5) with

$$\epsilon \widehat{Q}_k k^2 \Delta t = \alpha (k/N)^p. \tag{4.7}$$

Assuming Δt and ϵ are $\mathcal{O}(1/N)$, we obtain $\widehat{Q}_k = \mathcal{O}[(k/N)^{p-2}]$. Operator splitting generally adds an error of order $\mathcal{O}(\Delta t)$. However, since the contribution from the viscous step is smaller than that, it will not be an issue. We add an error $\mathcal{O}(k/N)^p$ per time step. Hence, we can hope to obtain an order of accuracy $\mathcal{O}(1/N)^p/\Delta t$ if the method is stable.

The numerical results in Figure 7 show that the exponentially filtered solution behaves much like—and in fact for small N's, outperforms—the SV solution of the Burgers' equation in Figure 2. However, the numerical experiments reported in Figure 8 indicate that EF does not necessarily converge to the entropy solution of nonconvex problems.

• *Rarefactions.* Computing solutions with rarefaction waves rely critically on sufficient dissipation to avoid unphysical shocks, and hence it should be checked that new schemes can handle such a case. As an example, we consider initial data

$$u_0(x) = 1 - \frac{1}{2}\text{sign}(x). \tag{4.8}$$

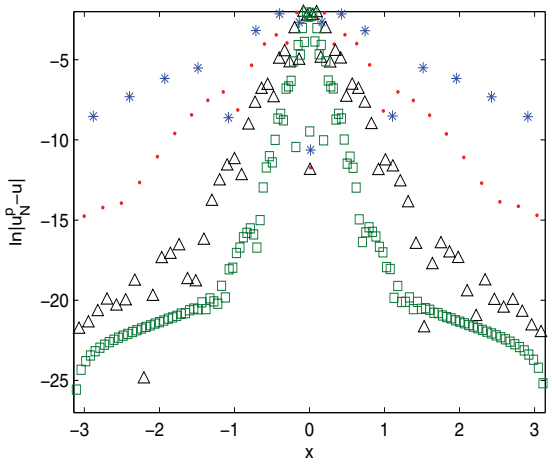

FIG. 7. *The exponentially filtered solution* (4.4) *of Burgers' equation, with* $\alpha = 10$ *and* $p = 6$. *This should be compared with the (A)SV solutions in Figure* 2.

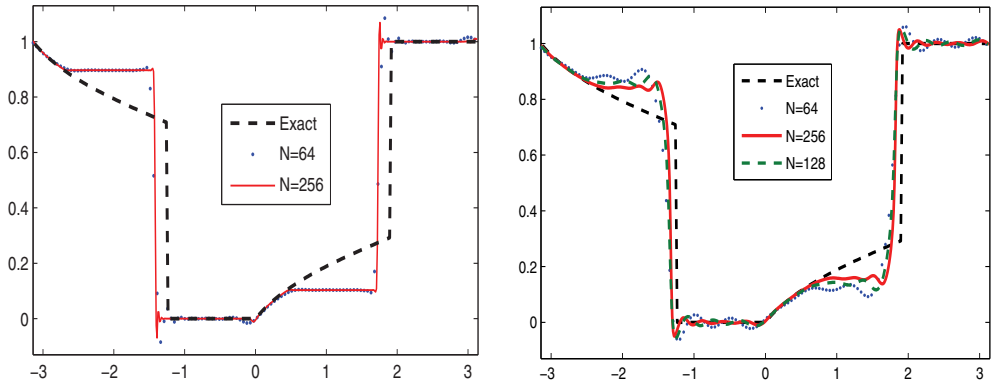

FIG. 8. *Left: The exponentially filtered solution* (4.4) *of the Buckley–Leverett Riemann problem with* $\alpha = 10$ *and* $p = 6$. *This should be compared with the (A)SV solutions in Figure* 6. *Similar results were obtained with the operator splitting version of the SV method, on the right, using SV step* (4.5) *with SV parameters* (4.3). *In either case, the SV variants converge to the entropy solution, whereas the EF solution does not.*

Results are shown in Figure 9. We find that both SV and ASV provide satisfactory results, while LSV shows some signs of instability in the rarefaction fan. These initial data also produce a shock wave, for which the schemes perform much like in the first example.

5. Numerical studies II. Systems of equations.

5.1. Shallow water equations. This fluid equation system has a quadratic pressure-like term and a source term that models bottom topography. It takes the form

$$\rho_t + (\rho u)_x = 0, \quad (\rho u)_t + \left(\rho u^2 + \frac{1}{2}\rho^2\right)_x = -\rho z_x, \tag{5.1}$$

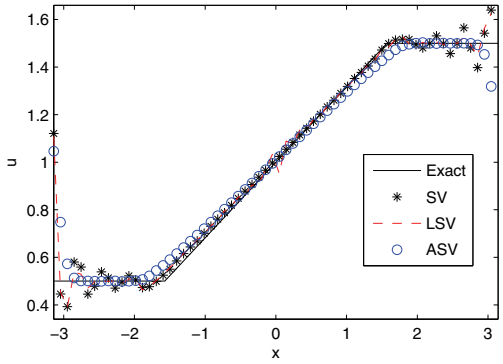

FIG. 9. *Burgers' equation rarefaction wave solution profiles.*

where z is a given bottom topography that is fixed, i.e., $z_t = 0$. As an example we consider

$$z(x) = \begin{cases} 0.1 \exp\left(\dfrac{x^2}{x^2 - 1.7^2}\right), & |x| < 1.7, \\ 0, & |x| \geq 1.7. \end{cases} \tag{5.2}$$

For initial data, the velocity u is set to zero, while $\rho + z$ jumps from 0.2 to 0.4 at $x = 0$. For the shallow water system, we need to make some modification to the localizer: First, note that it is enough to consider the mass density profile ρ for detecting the shocks of this system; hence we use $K(\rho_N)$. Obviously the resulting localizer needs to be properly normalized. In order to normalize, we simply divide $K(\rho_N)$ by the local value of ρ_N (before performing the modifications (2.2a)–(2.2c)).

The water height profiles ρ from ASV and SV at $N = 256$ are plotted in Figure 10. ASV smooths out the singularities somewhat, while SV shows a sharp profile with oscillations. As an error indicator, we show $\ln|\widetilde{u}_N|$, the absolute value of postprocessed velocity, logarithmically scaled, in Figure 11. The postprocessing was performed assuming the singularities were at -2.5, -0.6, 0.7, and 2.4. In the regions not yet affected by any waves, the exact solution is $u = 0$. We would want the schemes to retain at least fourth order accuracy in these regions. This expectation is confirmed sufficiently far from wave fronts, with ASV performing the best. The unprocessed velocity profiles at $N = 256$ are shown in Figure 11. It is interesting to note that SV and ASV primarily differ near the singularities before postprocessing.

5.2. Isothermal gas dynamics. As another example system we look at

$$\rho_t + (\rho u)_x = 0, \quad (\rho u)_t + (\rho u^2 + \rho)_x = 0. \tag{5.3}$$

We consider Riemann initial data with $u = 0$, and ρ jumping from 1 to 0.5 at $x = 0$, yielding two Riemann problems due to periodicity. The resulting velocity profiles from SV and ASV are shown in Figure 12. In the regions not yet affected by any waves, the exact solution for the velocity is $u = 0$. Therefore, as an error measure, we plot $\ln|\widetilde{u}_N|$ in Figure 13. The ASV scheme shows the best accuracy, especially at low resolutions. The postprocessing here is performed assuming the singularities are at 1, $\pi - 1$, -0.9, and $-\pi + 0.9$. We base the localizer on ρ in the same manner as described for the shallow water system above.

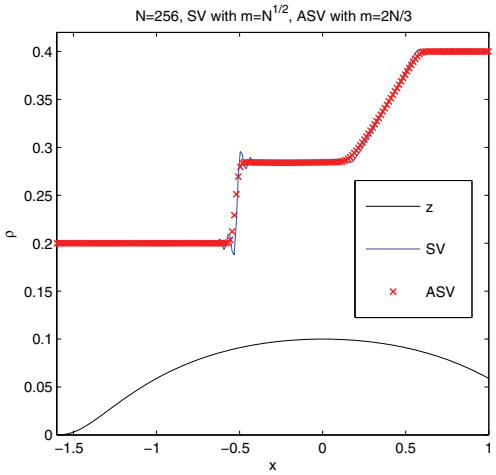

FIG. 10. *Shallow water problem. Water height for SV and ASV. z and $\rho + z$ are plotted.*

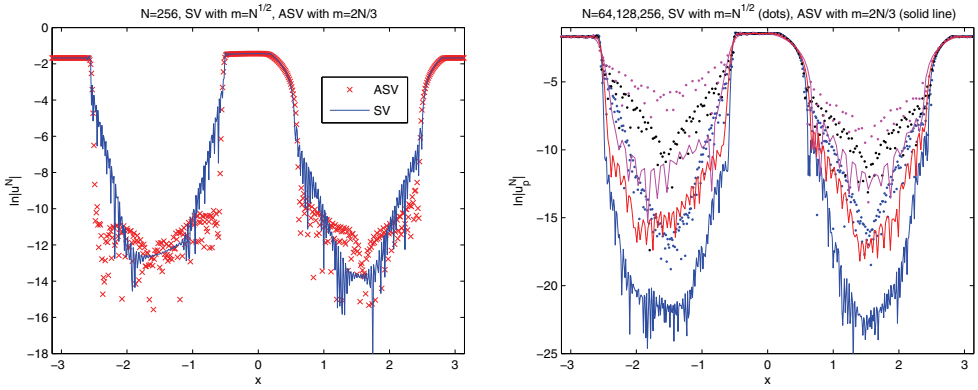

FIG. 11. *The shallow water problem. The velocity field for SV and ASV method preprocessed (left) versus postprocessed (right).*

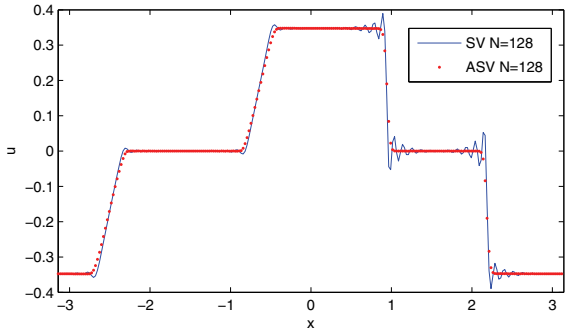

FIG. 12. *Velocity profiles for the isothermal Euler–Riemann problem. Solution sampled at $t = \pi/4$.*

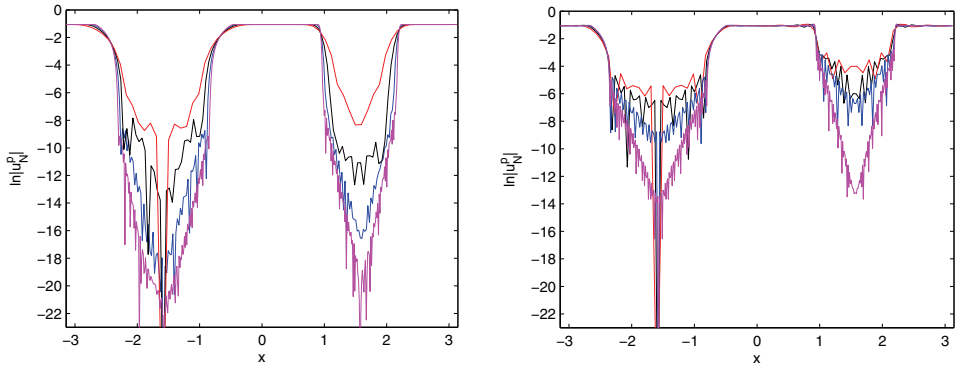

FIG. 13. $\ln|\widetilde{u}_N|$ *for the isothermal Euler–Riemann problem. ASV (left) and SV (right) solutions at* $N = 32, 62, 128,$ *and* 256. *Solution sampled at* $t = \pi/4$.

6. Conclusion. We introduced the new adaptive spectral viscosity (ASV) scheme (2.5). The scheme combines the high accuracy of the spectral viscosity (SV) method with stabilizing diffusion applied only at discontinuities. The discontinuity locations are found with the spectral edge detection algorithm of [3, 4, 20].

The ASV scheme (2.5) was tested numerically and compared to the standard SV method. We conclude that ASV offers significant improvement. In particular, for tests with Burgers' equation, isothermal gas dynamics, and shallow water with bottom topography, we obtained much better accuracy near the shock waves, and also significantly increased accuracy in the smooth regions. In particular, we observe a strong improvement at low resolutions. In addition to ASV, we also tested the new local viscosity (2.3) and local spectral viscosity (2.4) schemes. They appeared stable, yet convergence was sometimes slow, indicating that they do not feature enough viscosity to control the Gibbs' oscillations.

The Buckley–Leverett equation was used as a test case for treating scalar problems with nonconvex fluxes. The entropy solution to this problem is unique, but it is known that the convergence of various approximate methods to *the* entropy solution in this case may depend on sensitive parameterizations; otherwise, the approximations may converge to other weak solutions. The standard SV method had problems finding the entropy solution, although with sufficiently strong dissipation there appeared to be a slow convergence towards it. In contrast, the ASV method seems to be more robust, as it maintained high accuracy in the smooth regions also for the nonconvex case.

The ASV scheme may be implemented efficiently using FFT techniques. It is straightforward to augment existing implementations with ASV since one only has to add new terms to an existing code, rather than changing it.

REFERENCES

[1] A. MAJDA, J. MCDONOUGH, AND S OSHER, *The Fourier method for nonsmooth initial data*, Math. Comp., 32 (1978), pp. 1041–1081.

[2] G.-Q. CHEN, *Compactness methods and nonlinear hyperbolic conservation laws*, in Some Current Topics on Nonlinear Conservation Laws, AMS/IP Stud. Adv. Math. 15, Amer. Math. Soc., Providence, RI, 2000, pp. 34–75.

[3] A. GELB AND E. TADMOR, *Detection of edges in spectral data*, Appl. Comput. Harmo. Anal., 7 (1999), pp. 101–135.

[4] A. GELB AND E. TADMOR, *Detection of edges in spectral data* II. *Nonlinear enhancement*, SIAM J. Numer. Anal., 38 (2000), pp. 1389–1408.

[5] A. Gelb and E. Tadmor, *Enhanced spectral viscosity approximations for conservation laws*, Appl. Numer. Math., 33 (2000), pp. 3–21.
[6] D. Gottlieb and E. Tadmor, *Recovering pointwise values of discontinuous data within spectral accuracy*, in Progress and Supercomputing in Computational Fluid Dynamics, Proceedings of U.S.-Israel Workshop, Progr. Sci. Comput. 6, Birkhäuser Boston, Boston, MA, 1985, pp. 357–375.
[7] S. Gottlieb, C.-W. Shu, and E. Tadmor, *Strong stability-preserving high-order time discretization methods*, SIAM Rev., 43 (2001), pp. 89–112.
[8] B.-Y. Guo, H.-P. Ma, and E. Tadmor, *Spectral vanishing viscosity method for nonlinear conservation laws*, SIAM J. Numer. Anal., 39 (2001), pp. 1254–1268.
[9] B. T. Hayes and P. G. LeFloch, *Non-classical shocks and kinetic relations: Scalar conservation laws*, Arch. Rational Mech. Anal., 139 (1997), pp. 1–56.
[10] H. Li, H.-P. Ma, and E. Tadmor, *Hyper Spectral Viscosity Method for Nonlinear Conservation Laws*, unpublished note, 1999.
[11] Y. Maday, S. M. Ould Kaber, and E. Tadmor, *Legendre pseudospectral viscosity method for nonlinear conservation laws*, SIAM J. Numer. Anal., 30 (1993), pp. 321–342.
[12] Y. Maday and E. Tadmor, *Analysis of the spectral vanishing viscosity method for periodic conservation laws*, SIAM J. Numer. Anal., 26 (1989), pp. 854–870.
[13] E. Panov, *Uniqueness of the solution of the Cauchy problem for a first-order quasilinear equation with an admissible strictly convex entropy*, Mat. Zametki, 55 (1994), pp. 116–129 (in Russian); translation in Math. Notes, 55 (1994), pp. 517–525.
[14] S. Schochet, *The rate of convergence of spectral-viscosity methods for periodic scalar conservation laws*, SIAM J. Numer. Anal., 27 (1990), pp. 1142–1159.
[15] C.-W. Shu and P. S. Wong, *A note on the accuracy of spectral method applied to nonlinear conservation laws*, J. Sci. Comput., 10 (1995), pp. 357–369.
[16] E. Tadmor, *Convergence of spectral methods for nonlinear conservation laws*, SIAM J. Numer. Anal., 26 (1989), pp. 30–44.
[17] E. Tadmor, *Shock capturing by the spectral viscosity method*, Comput. Methods Appl. Mech. Eng., 80 (1990), pp. 197–208.
[18] E. Tadmor, *Super viscosity and spectral approximations of nonlinear conservation laws*, in Numerical Methods for Fluid Dynamics. 4. Proceedings of the International Conference held at the University of Reading, Reading, April 1992, M. J. Baines and K. W. Morton, eds., The Clarendon Press, Oxford University Press, New York, 1993, pp. 69–81.
[19] E. Tadmor, *Total variation and error estimates for spectral viscosity approximations*, Math. Comp., 60 (1993), pp. 245–256.
[20] E. Tadmor, *Filters, mollifiers and the computation of the Gibbs phenomenon*, Acta Numer., 16 (2007), pp. 305–378.
[21] E. Tadmor and J. Tanner, *Adaptive mollifiers for high resolution recovery of piecewise smooth data from its spectral information*, Found. Comput. Math, 2 (2002), pp. 155-189.
[22] E. Tadmor and J. Tanner, *An adaptive order Godunov type central scheme*, in Proceedings of the 9th International Conference in Hyperbolics Problems: Theory, Numerics, Applications (Pasadena, 2002), Springer, Berlin, 2003, pp. 871–880.
[23] E. Tadmor and J. Tanner, *Adaptive filters for piecewise smooth spectral data*, IMA J. Numer. Anal., 25 (2005), pp. 635–647.
[24] L. Tartar, *The Compensated Compactness Method for a Scalar Hyperbolic Equation*, Carnegie Mellon University Lecture Notes, 1987.